Properties of Undoped and Ca-Doped $LaMnO_3$ − Non-Stoichiometry and Defect Structure

Mondher Yahia[a] and Habib Batis*[a]

Keywords: Non-stoichiometry / Perovskites / Preparation

Oxygen-excessive $LaMnO_{3+y}$ samples with $0.02 \leq y \leq 0.26$ have been prepared by thermal decomposition in air at 450 °C of a precursor obtained from an aqueous solution of lanthanum nitrate and manganese acetate (atomic ratio La/Mn = 1). The obtained solid is annealed at different temperatures from 700 to 1000 °C and under three oxygen pressures: 1.00, 0.21, and 10^{-4} atm. Samples with $0.14 \leq y \leq 0.26$ are simple-phased rhombohedral perovskites, the distortion of which decreases as the oxygen content (and Mn^{4+} content) increases. Samples with $0.02 \leq y \leq 0.09$, obtained under low oxygen pressure (10^{-4} atm), have orthorhombic symmetry. In this case, the order of lattice parameters $c/\sqrt{2} < a < b$, characteristic of O′-perovskites, is a consequence of the Jahn–Teller distortion of the oxide octahedron around the d^4 Mn^{4+} cation. The volume (V_f) per $LaMnO_{3+y}$ formula unit decreases regularly with increasing oxygen content (i.e., oxidation). Study has shown that the oxygen content is best described in terms of La and Mn vacancies, rather than of interstitial anions. Density measurements confirm the cation vacancy model involving equal amounts in La and Mn sublattices. The infrared spectra of $LaMnO_{3+y}$ samples have been interpreted in connection with the structures of these solids. Correlations have been established between the spectral evolution and the crystal distortion of these compounds. $La_{1-x}Ca_xMnO_{3\pm y}$ oxides with $0 < x \leq 1$ have been synthesised by the same route, at 700 °C and under an oxygen pressure of 0.21 atm. It is shown that a negative correlation exists between the calcium content *x* and the degree of non-stoichiometry: at low Ca content, the oxygen content is higher. The ability to form over-stoichiometric compounds in air decreases with increasing Ca content and mostly disappears at $x \geq 0.7$. Samples with $0.1 \leq x \leq 0.4$ are simple-phased rhombohedral perovskites with constant Mn^{3+}/Mn^{4+} ratios. Samples with $0.5 \leq x \leq 1$ have orthorhombic symmetry. In this case, a linear variation of the Mn^{4+} content as a function of the Ca content is observed. The defect structure of these compounds is described in terms of La and Mn vacancies when $0 < x \leq 0.7$ ($0 \leq y \leq 0.19$) and anion vacancies when $0.8 \leq x \leq 1$ ($-0.04 \leq y < 0$).

Introduction

Perovskite-type oxides can be represented as ABO_3, where B is a transition cation of the 3d, 4d, or 5d group and A is either a lanthanide (generally La, but sometimes Ce, Pr, or Nd) or an alkaline earth metal (Ca, Sr, or Ba). In the crystal structure, the A ion is coordinated by twelve oxygen ions, which in turn belong to eight BO_6 octahedrons sharing corners. The stability, derived primarily from the Madelung energy of the stacking of rigid BO_6 octahedrons, requires that B be a cation with a preference for octahedral coordination. The A ion occupying the large dodecahedral interstice has to have an appropriate size.[1−3]

They have been studied for their physical characteristics, such as ferroelectricity, piezoelectricity, magnetism, superconductivity at high temperature etc. During the last two decades they have been consistently proposed as alternative catalysts for reactions involving hydrogen, such as hydrogenolysis of hydrocarbons[4] as well as for reaction combustion of carbon monoxide and light hydrocarbons.[5−11]

The great variety of A and B ions able to take part in the structure, the possibility of changing the valence of the B ion by proper selection of A and also the partial substitution of cations to form compounds of formula $(AA')(BB')O_3$ make feasible the preparation of perovskites with very specific properties.

Lanthanum manganite oxides of formula $LaMnO_{3+y}$, exhibit non-stoichiometry on one or more sub-lattices.[12] The opinion is widely shared that the oxygen excess is partially compensated by the oxidation of Mn^{3+} (d^4) to Mn^{4+} (d^3) in the B sub-lattice. Consequently, it can be seen that the Jahn−Teller effect of Mn^{3+} ions, and hence the structure distortion, will decrease with increasing number of Mn^{4+} ions. In fact, there are two characteristic distortions that influence the perovskite structure of manganites. One consists of co-operative tilting of MnO_6 octahedrons. This kind of distortion is a consequence of the ionic radii and is common in perovskites with small central cations (Goldschmidt factor $t < 1$). The other kind of structure distortion is associated with the Jahn−Teller effect of Mn^{3+} ions, resulting

[a] Laboratoire d'Études de Solides Catalyseurs, Département de Chimie, Faculté des Sciences de Tunis,
1060 Tunis, Tunisie

  DOI: 10.1002/ejic.200300025

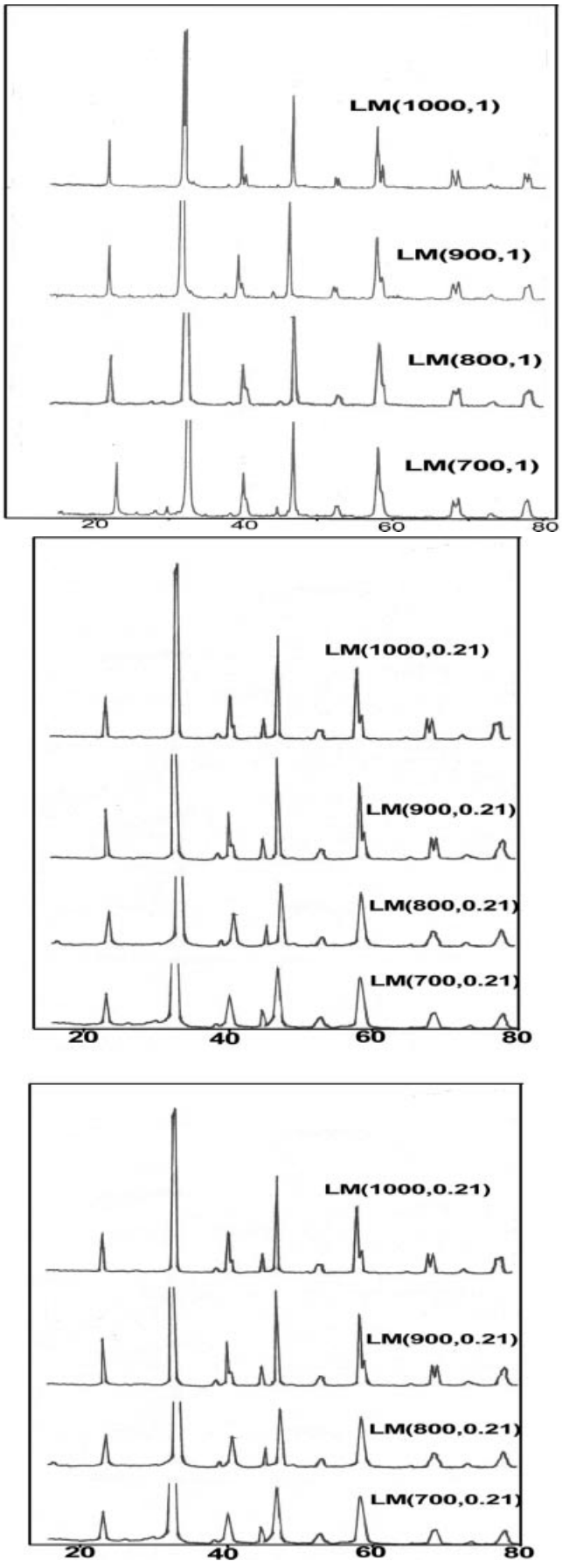

Figure 1. XRD diagrams of LM(*T*,*P*) samples

in the distortion of $Mn^{3+}O_6$ octahedrons and their co-operative ordering below a certain critical temperature. Despite the extensive literature on non-stoichiometric manganite perovskites, a detailed and systematic investigation over a wide range of y values to delineate the stability region of the homogeneous phase in the $LaMnO_{3+y}$ system is still lacking. As well as the non-stoichiometric $LaMnO_{3+y}$ family, Mn^{4+} ions can also be introduced into compounds of general formula $La_{1-x}C_xMnO_{3+y}$ by substitution of La^{3+} by a divalent ion (C = divalent cation, usually an alkaline earth). Such compounds have been extensively studied,[13−18] due to their potential for application as air electrodes in high-temperature solid oxide fuel cells. In the case of Sr-doped $LaMnO_3$, the range of concentration x is limited by the larger size of Sr^{2+} in relation to that of the La^{3+} ion. Given the importance of C content on the Mn^{3+}/Mn^{4+} ratio and therefore on the defect structure, it seems appropriate to consider the related system $La_{1-x}Ca_xMnO_{3\pm y}$ and to acquire knowledge of its defect structure over the whole range of concentrations ($0 \leq x \leq 1$).

The objectives of this study are:

(i) to prepare, by a simple and reproducible route, $LaMnO_{3+y}$ and $La_{1-x}Ca_xMnO_{3\pm y}$ compounds over a wide range of y and x values,

(ii) to determine their phase stabilities and oxygen non-stoichiometries,

(iii) to determine the best model for their defect chemistry,

(iiii) to study the effect of Mn^{4+} content on the frequency of Mn−O characteristic infrared absorption bands in undoped and in Ca-doped lanthanum manganites.

Results

1-LM(*T*,*P*) Oxides

The diffraction patterns of the LM(*T*,*P*) compounds were closely related to the patterns that would be expected of simple perovskite structures. Differences between the ideal

Table 1. Crystallographic parameters of LM(*T*,*P*) oxides

T [°C]	Symmetry	*a* [Å]	*b* [Å]	*c* [Å]	V_f [Å^3]	y
$P = 10^{-4}$ atm						
700	ortho. *Pbnm*	5.55(2)	5.63(2)	7.75(3)	60.55	0.09
800	ortho. *Pbnm*	5.54(2)	5.65(1)	7.78(3)	60.83	0.06
900	ortho. *Pbnm*	5.57(2)	5.69(1)	7.74(2)	61.33	0.03
1000	ortho. *Pbnm*	5.57(2)	5.72(1)	7.72(3)	61.50	0.02
$P = 0.21$ atm						
700	hex. $R\bar{3}c$	5.508(5)	−	13.39(3)	58.63	0.24
800	hex. $R\bar{3}c$	5.512(5)	−	13.38(3)	58.67	0.21
900	hex. $R\bar{3}c$	5.519(4)	−	13.35(2)	58.73	0.16
1000	hex. $R\bar{3}c$	5.525(3)	−	13.37(1)	58.92	0.14
$P = 1$ atm						
700	hex. $R\bar{3}c$	5.516(3)	−	13.33(1)	58.57	0.26
800	hex. $R\bar{3}c$	5.520(3)	−	13.32(1)	58.58	0.23
900	hex. $R\bar{3}c$	5.524(3)	−	13.33(1)	58.72	0.17
1000	hex. $R\bar{3}c$	5.528(5)	−	13.39(3)	59.07	0.16

and observed patterns were the split reflections, implying distortions of the lattice from cubic symmetry (Figure 1). The XRD patterns of LM(T,0.21) and LM(T,1) oxides were refined in the space group $R\bar{3}c$, hexagonal description (Z = 6). Those of LM(T,10^{-4}) were refined in the *Pbnm* space group, orthorhombic description (Z = 4). The unit cell parameters determined after the refinement as well as the volume per unit formula (V_f) and oxygen contents (y) of the samples are listed in Table 1.

Mn−O distances were determined, taking those perovskites $LaNiO_3$[19] and $GdFeO_3$[20] exhibiting $R\bar{3}c$ and *Pbnm* space groups, respectively, as starting models. For $LaNiO_3$, La atoms are at 6a (0,0,$^1/_4$); Mn at 6b (0,0,0); and O at 18e (x,0,$^1/_4$) with $x \approx 0.547$. For $GdFeO_3$, La atoms are at 4c (x,y,$^1/_4$) with $x \approx 0.984$, $y \approx 0.063$; Mn at 4b (0,$^1/_2$,0); O1 at 4c with $x \approx 0.1005$, $y \approx 0.4672$ and O2 at 8d (x,y,z) with $x \approx 0.6957$, $y \approx 0.3016$, $z \approx 0.0506$.

Figure 2 shows the plot of unit formula volume (V_f) vs. y. A net decrease in the volume is observed as the oxygen content increases. This effect can be correlated with the increasing content of Mn^{4+} (= $2y$), which is smaller than Mn^{3+} [21] The presence of smaller cations in the B sublattice of the ABO_3 perovskite is responsible both for the reduction in unit cell volume and for the increase in the Goldschmidt tolerance factor[22] ($t = d_{A-O}/\sqrt{2}d_{B-O}$), hence the decrease of the rhombohedral distortion of the lattice. In contrast, for small y values (hence low Mn^{4+} concentrations), a more distorted structure is favoured, as observed for LM(T,10^{-4}) oxides, which show orthorhombic symmetry. In this case, the order of lattice parameters $c/\sqrt{2} < a < b$, characteristic of O′-perovskites,[3] is a consequence of the Jahn−Teller distortion of the oxide octahedron around the d^4 Mn^{3+} cation. A region of non-stoichiometry $0 < y < 0.15$ for $LaMnO_{3+y}$ was reported by Wold and Arnott,[23] with a change in symmetry (at room temperature) from orthorhombic to rhombohedral for an Mn^{4+} concentration greater than 21% ($LaMnO_{3.105}$), which closely agrees with our observation. The rhombohedral symmetry was observed even for the samples with the highest Mn^{4+} contents, as clearly shown by the characteristic splitting of the diffraction peaks (Figure 1). Moreover the rhombohedral angles of these samples are still considerably larger than 60° (which corresponds to cubic symmetry): α_r = 60.6°, for instance, for sample LM(700,1), with 52% Mn^{4+}. A sample of composition $LaMnO_{3.2}$ reported by Tofield and Scott[24] also showed a rhombohedral symmetry with an angle α_r = 60.3°.

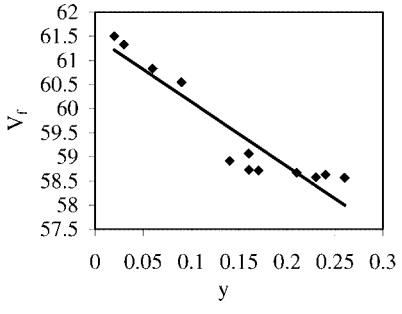

Figure 2. Variation of unit formula volume V_f with excess oxygen content y

To evaluate the nature of defects in LM(T,P) oxides, experimental density values were compared to those of five models of defect distribution in the lattice previously reported by Van Roosmalen et al.[25] For each of these models, the calculated density is defined by $d = M/N \cdot V_f$, where M is the molar mass of the formula unit, V_f is the formula unit volume, and N is the Avogadro constant. The variation of V_f as a function of y was derived from Figure 2. $V_f = (61.53 - 13.88 \cdot y)$ Å^3. The density calculated as a function of y for the five models, together with the experimentally determined densities obtained for LM(T,P) samples are reported in Table 2.

Table 2. Theoretical and experimentally determined density values [g·cm^{-3}] as a function of y

y	O_i[a]	V_{Mn}[b]	V_{La} and V_{Mn}[c]	V_{La}[d]	V_{La} and V_O[e]	ρ_{exp}
0.26	7.05	6.66	6.49	6.24	6.12	6.55(2)
0.24	7.01	6.65	6.49	6.26	6.08	6.54(2)
0.23	6.99	6.64	6.49	6.28	6.06	6.56(2)
0.21	6.94	6.64	6.49	6.30	6.02	6.54(2)
0.17	6.86	6.61	6.49	6.34	5.95	6.55(2)
0.16	6.84	6.60	6.49	6.35	5.93	6.55(2)
0.14	6.80	6.59	6.50	6.38	5.89	6.53(2)
0.09	6.70	6.57	6.50	6.43	5.80	6.53(2)
0.06	6.64	6.55	6.51	6.46	5.75	6.52(2)
0.03	6.58	6.54	6.52	6.49	5.70	6.53(2)
0.02	6.56	6.53	6.52	6.50	5.68	6.51(2)

[a] $LaMnO_3O_{i,y}$ (O interstitial). [b] $LaMn_{(3-2y/3)}O_3$ (Mn vacancies). [c] $La_{3/3+y}V_{La,y/3+y}Mn_{3/3+y}V_{Mn,y/3+y}O_3$ (La and Mn vacancies). [d] $La_{1-2y/3}V_{La,2y/3}MnO_3$ (La vacancies). [e] $La_{0.8}MnO_{2.7+y}$ (La and O vacancies).

From the agreement between the observed and calculated densities, it is obvious that an equal distribution of concentrations of Mn and La vacancies in cationic sub-lattices is the predominant defect model. The analysis results, which show an atomic ratio La/Mn = 1, are in good agreement with this proposed model.

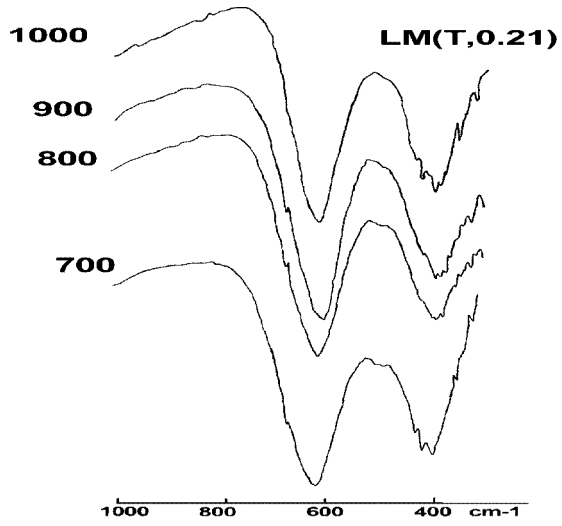

Figure 3. IR spectra of LM(T,0.21) samples

Table 3. Higher frequency band as a function of y

y	0.24	0.21	0.16	0.14	0.09	0.06	0.03	0.02
ν_1 [cm^{-1}]	618	612	610	604	597	594	589	577
d_{MnO} [Å]	1.959	1.961	1.963	1.966	2.010[a]	2.012[a]	2.016[a]	2.018[a]
$r_{Mn_x}+ r_O$ [Å][b]	1.995	2.001	2.011	2.015	2.025	2.031	2.038	2.040
Δ [Å]	−0.036	−0.040	−0.048	−0.049	−0.015	−0.019	−0.022	−0.022

[a] Average value of three Mn−O distances due to Jahn−Teller deformation. [b] r_{Mn} is the Mn site radius defined by: $r_{Mn} = [3\cdot(1 - y)]/(3 + y)\cdot r_{Mn^{3+}} + 6y/(3 + y)\cdot r_{Mn^{4+}} + y/(3 + y)\cdot r_V$, where r_V is the radius of a vacancy, taken equal to 0.60 Å[24] and $r_{Mn^{3+}} = 0.65$ Å; $r_{Mn^{4+}} = 0.54$ Å.

All samples showed similar types of IR spectra. As an example, Figure 3 shows the IR spectra of LM(T,0.21) samples. Two absorption bands, at 800−550 and 450−300 cm^{-1}, were observed in each spectrum. The higher frequency band extends from about 800 to 500 cm^{-1}. Its absorption maximum decreases progressively with increasing y values (Table 3). The lower frequency band extends from about 475 cm^{-1} to the limit of the available experimental range at about 300 cm^{-1}, with a centre at 380 cm^{-1}.

IR spectra of ABO_3 perovskite oxides have been studied by several workers.[26−29] In general, the ABO_3 perovskites show two prominent bands in the 1000−300 cm^{-1} spectral region. The assignment of absorption bands by factor group analysis in these oxides has not been as successful as in fluorides[29−32]; in an ABO_3 perovskite of cubic symmetry there should be three sets of triply degenerate infrared-active modes of symmetry F_{1u} and one inactive mode of symmetry F_{2u}. This F_{2u} mode, however, can become active through distortion of the crystal lattice from the ideal cubic structure. The perturbation needs only be slight and would of course split the degeneracies in all modes. Fair success has been obtained by considering the internal modes of the BO_3 octahedron and the external ones of the A−(BO_3) groups. In the discussion of the vibration nature of the BO_3 group, it is considered to be arranged as central B atom octahedrally surrounded by six O half-atoms. Nakagawa et al.[30] therefore assigned the ν_1 mode to the B−O stretching normal vibration where the motion is primarily that of a change in the length of the B−O bond. Two modes − ν_2 and ν_4 − were assigned to the B−O bending normal vibration, where the motion is that of a change in the O−B−O bond angle. Both the relative magnitude and the sign of the displacements will depend on the bond-force constants and relative masses of the atoms. Moreover, the frequency of these bands has been related to the strength of the metal−oxygen covalency.[26] A fourth mode − ν_3 − was assigned to the A−(BO_3) vibration. The stretching vibration would be expected to occur at frequencies higher than the bending vibration, from comparison of the change in potential energy due to repulsive forces between ions in the two normal vibrations.

Infrared absorption bands in the vicinities of 600 and 400 cm^{-1} were observed for the various manganites investigated. The higher frequency band ν_1 was assigned to the Mn−O stretching normal vibration and the lower band ν_2 to the Mn−O bending vibration. Detailed analysis of distorted $LaMnO_{3+y}$ spectra showed additional bands, probably due to systematic distortion from ideal cubic symmetry to the orthorhombic structure for LM(T,10^{-4}) and to the rhombohedral structure for LM(T,0.21) and LM(T,1), which would split degenerate modes to give additional distinct frequencies. Spectra are given in Figure 4 to illustrate the importance of cell deformation for the number, shape, and position of IR bands.

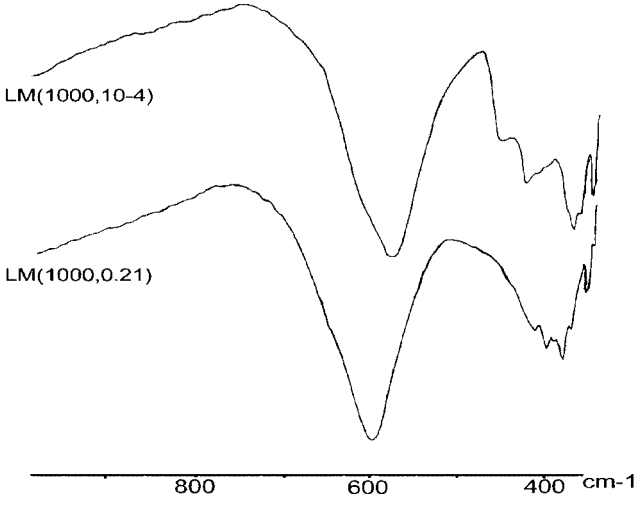

Figure 4. IR spectra of LM(1000,0.21) and LM(1000,10^{-4}) samples

Table 3 gives the vibrational frequencies of the M−O (ν_1) bond together with d_{Mn-O} distances as a function of non-stoichiometry y, which measures Mn^{4+} concentration in the MnO_3 sub-lattice. It can be seen that ν_1 decreases with decreasing y and increasing d_{Mn-O} distances.

2-LCMx(*T*,*P*) Oxides

All samples ($0 \leq x \leq 1$) were obtained after treatment under air at 700 °C. The diffraction patterns are given in Figure 5. X-ray powder diffraction patterns of all samples were completely indexed as the perovskite-type structure and showed the absence of simple oxides such as La_2O_3, Mn_2O_3, MnO_2, and CaO over the whole range of x values. The maximum incorporation rate seems to be influenced by the ionic radius of the substituted cation. Indeed, in the $LaMnO_3$ type of perovskite structure, the coordination number of La^{3+} ions is 12 with an ionic radius of 1.36 Å, and that of Ca^{2+} in the same site is 1.34 Å,[23] smaller than that of other alkaline metal ions such as Sr^{2+}. Thus, it is to

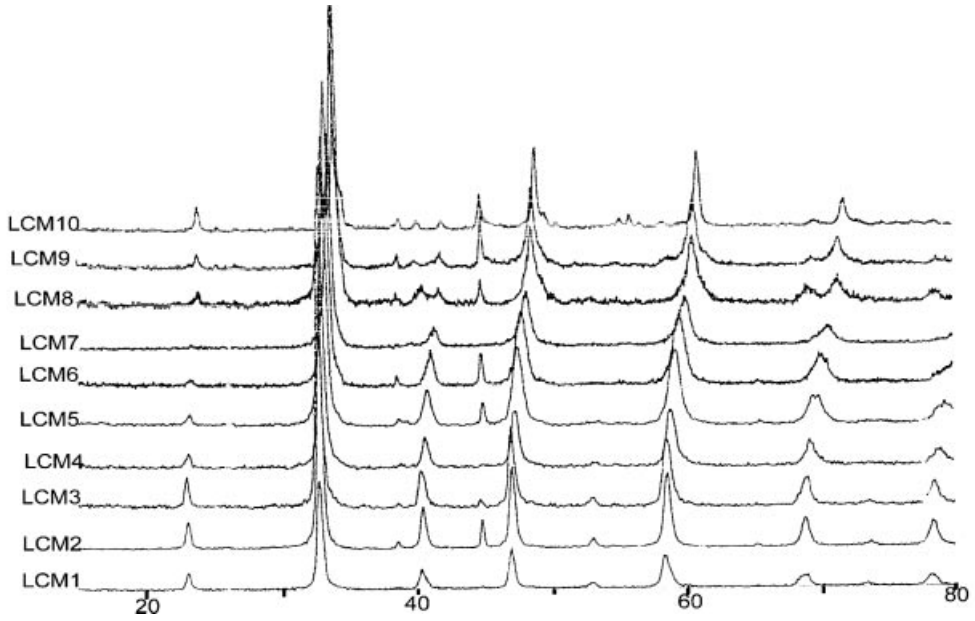

Figure 5. XRD diagrams of LCMx samples

Table 4. Crystallographic parameters of LCMx oxides

LCMx	Symmetry	a [Å]	b [Å]	c [Å]	V_f [Å^3]	Ca/Mn	O/Mn	Mn^{4+} (%)	d [g·cm^{-3}]
LCM1	hexag. $R\bar{3}c$	5.492(6)	–	13.34(6)	58.08	0.11(2)	3.19(2)	49	6.29
LCM2	hexag. $R\bar{3}c$	5.488(5)	–	13.27(5)	57.70	0.21(2)	3.14(2)	49	–
LCM3	hexag. $R\bar{3}c$	5.483(7)	–	13.28(7)	57.58	0.30(2)	3.10(2)	50	5.94
LCM4	hexag. $R\bar{3}c$	5.450(3)	–	13.43(5)	57.57	0.39(2)	3.06(2)	51	–
LCM5	ortho. *Pbnm*	5.36(4)	7.69(1)	5.46(1)	56.26	0.50(2)	3.05(2)	60	5.55
LCM6	ortho. *Pbnm*	5.36(2)	7.65(1)	5.40(2)	55.35	0.60(2)	3.03(2)	66	–
LCM7	ortho. *Pbnm*	5.33(2)	7.57(1)	5.37(2)	54.16	0.70(2)	3.00(2)	70	5.25
LCM8	ortho. *Pbnm*	5.36(6)	7.39(3)	5.40(5)	53.47	0.79(2)	2.99(2)	77	–
LCM9	ortho. *Pbnm*	5.31(3)	7.37(3)	5.39(4)	52.73	0.90(2)	2.97(2)	84	4.82
LCM10	ortho. *Pbnm*	5.34(3)	7.33(3)	5.30(3)	51.86	1.00(2)	2.96(2)	92	4.52

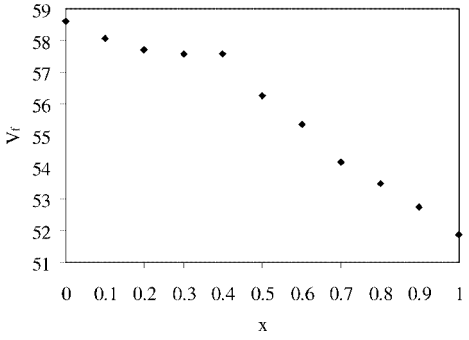

Figure 6. Variation of unit formula volume V_f with substitution level x

be expected that the limit of substitution of Ca^{2+} in $LaMnO_3$ should be much higher than that reported for Sr^{2+} ($x = 0.6$).

The influence of the calcium content on the perovskite-type structure is clearly shown by the evolution of the number and the profile of XRD peaks (Figure 5). For $0 \leq x < 0.5$, the XR diffraction diagrams are similar to those of LM(T,0.21) samples and so are indexed in the same space group (i.e., $R\bar{3}c$). For higher x values the splitting and broadening of XRD are indicative of lower symmetry. Therefore, for $0.5 \leq x \leq 1$, the diffraction patterns are indexed in space group *Pbnm*, orthorhombic description. The lattice parameter determined from XRD patterns of LCMx samples together with unit formula volume V_f, density, and atomic ratios are listed in Table 4.

Ca incorporation induces a cell contraction, as shown by the decrease in V_f when the substitution rate increases (Figure 6). Analysis results show that the atomic Ca/Mn ratio is almost equal to the theoretical value x while the O/Mn ratio decreases from 3.19 (for $x = 0.1$) to 2.96 (for $x = 1$). As in the case of $LaMnO_{3+y}$, experimental densities were determined for (La,Ca)$MnO_{3\pm y}$ and listed in Table 4.

The experimentally ascertained density value for each sample was compared to those of the previously discussed five models of defect distribution in the lattice. Two models were retained to describe the defect chemistry in

(La,Ca)$MnO_{3\pm y}$. The first, Mn and La vacancies in equal concentrations, described the observed results well for $x \leq 0.7$. The second, with anion vacancies, described experimental results well for $x > 0.7$. Theoretical and experimental values are reported in Figure 7.

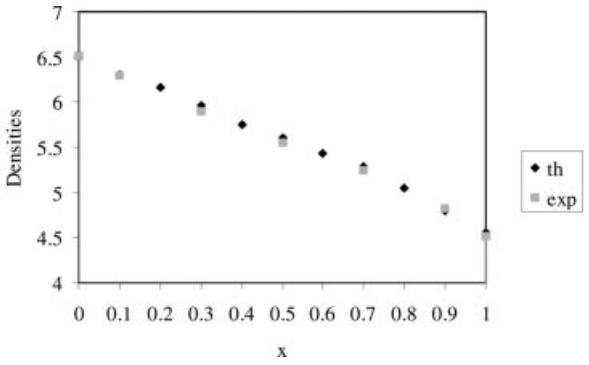

Figure 7. Theoretical (th) and experimentally determined (exp) densities of LCMx as a function of x

The oxygen non-stoichiometry y and the Mn^{4+} content are reported in Figure 8 as a function of Ca content x. The oxygen content y decreases with increasing x from $y = 0.24$ (for $x = 0$) to $y = -0.04$ (for $x = 1$). The Mn^{4+} concentration is constant for $0 \leq x \leq 0.4$ and increases almost linearly with increasing x for $0.5 \leq x \leq 1$.The maximum value, 0.92, for $x = 1$ shows that $CaMnO_{2.92}$ sample is in a reduced state. IR spectra of LCMx oxides (Figure 9) showed two absorption bands.

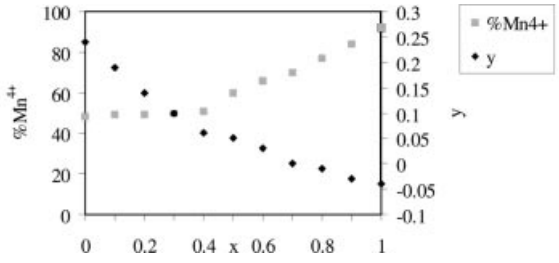

Figure 8. Variation of Mn^{4+} concentration and oxygen excess y with substitution level x in LCMx samples

The profiles of these bands changed with the substitution rate x. The higher frequency band, ν_1, was observed in the vicinity of 605 cm^{-1} for $x \leq 0.4$. For $0.5 \leq x \leq 1$, this band became asymmetric, with a high-frequency tail and extended from about 800 to 500 cm^{-1}. Its half-width increased from 90 to 180 cm^{-1}.The second band, of lower frequency, was initially centred at 380 cm^{-1} with shoulders at 392, 384, and 368 cm^{-1}. As x increased, this band broadened, shifted to somewhat higher frequencies and exhibited additional fine structure in the spectral range 350−520 cm^{-1}. For $x = 1$, the spectrum showed absorption bands in the 700−350 cm^{-1} region. In the spectral range of the ν_1 absorption mode, two bands were observed at 700 and 605 cm^{-1}. The lower frequency bands − at 514, 458, 421, 378, and 372 cm^{-1} − were in the spectral range of the ν_2 and

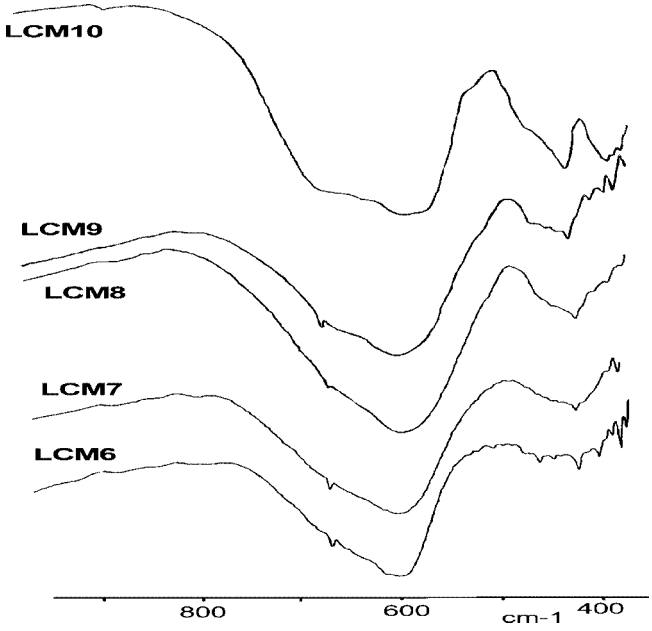

Figure 9. IR spectra of LCMx samples

ν_4 absorption modes of MnO_3 groups. Their splitting, in comparison to absorption bands in LCMx ($x \leq 0.4$) spectra, was indicative of an additional distortion of LCMx ($x \geq 0.5$) perovskite structures.

Discussion

$LaMnO_{3+y}$ oxides have been prepared as monophased perovskite structures from aqueous solutions of lanthanum nitrate $La(NO_3)_3{\cdot}6H_2O$ and manganese acetate $Mn(CH_3COO)_3$. The excess oxygen content y varied in a large range between 0.02 and 0.26. This was dependent of treatment, temperature and oxygen pressure. The y values thus decreased with increasing temperature and decreasing oxygen pressure. This tendency seemed to be confirmed under high oxygen pressures (200 atm) with a limiting y value of 0.31[33] Values comparable to $y = 0.26$ have been obtained by other preparation routes such as the sol-gel[34,35] and citrate methods[33] and calcination under an oxygen stream (1 atm).

XRD patterns showed a deviation from that of an ideal cubic structure. The splitting of peaks increased as the oxygen pressure of final treatment decreased. XRD patters were performed in the space group *Pbnm* ($Z = 4$), orthorhombic description for $y \leq 0.09$ ($[Mn^{4+}] \leq 18\%$), and in the space group $R\bar{3}c$ ($Z = 6$), rhombohedral description for $y \geq 0.14$ ($[Mn^{4+}] \geq 28\%$). The order, $c/\sqrt{2} < a < b$, of LM(T,10^{-4}) solids (orthorhombic structure), characteristic of O′-perovskites, is a consequence of the Jahn−Teller distortion of the oxide octahedron around the d^4 Mn^{3+} cation.[36] Long-range Jahn−Teller distortion is reduced when oxidation of some Mn^{3+} to Mn^{4+} occurs in $LaMnO_{3+y}$ with $y > 0.09$. There is a difference with the results ob-

tained by Hervieu et al.[37] and Verelest et al.,[34] who observed the formation of a cubic phase for $LaMnO_{3.165}$ oxide ($[Mn^{4+}] = 33\%$). In our case we observe rhombohedral symmetry even for the samples with higher Mn^{4+} contents, as clearly shown by the characteristic splitting of the diffraction peaks. Such splitting could be masked by a lack of crystallinity in the samples.

From the quoted cell parameters, we find the volume per unit formula V_f to decrease with increasing oxidation from 61.50 Å^3 for $y = 0.02$ ($[Mn^{4+}] = 4\%$) to 58.92 Å^3 for $y = 0.26$ ($[Mn^{4+}] = 52\%$). This tendency is also observed when oxidation to Mn^{4+} is partially compensated by the substitution of La^{3+} cations by Ca^{2+} in $La_{1-x}Ca_xMnO_{3\pm y}$ (Figure 10). In this case, V_f decreases to 51.86 Å^3 for $x = 1$. There is a good agreement between our V_f values and those reported in the literature for different oxygen stoichiometries, such as $LaMnO_{3.12}$[24] and $LaMnO_{3.158}$,[25] which interpolate well in Figure 10.

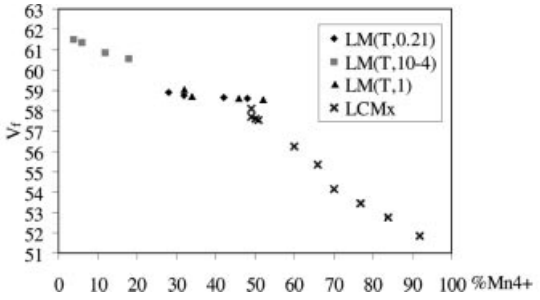

Figure 10. Variation of unit formula volume of LM and LCMx with Mn^{4+} content

The continuity in V_f vs. y variation between undoped and Ca-doped $LaMnO_3$ samples suggests that the symmetry of the manganite structure is largely determined by the concentration of Mn^{4+} ions. This is probably related to the mechanism of incorporation of the excess oxygen. The models involving vacancies either in cation or anion sublattices rather than oxygen interstitials were proposed as the predominant defects. This defect distribution in LM and LCMx solids, may be expressed by Kröger−Vink notations:[38]

LM samples:

$$LaMnO_3 + {}^{y}/_{2}\cdot O_2 \rightleftarrows LaV_{y/3}'''Mn_{1-2y}Mn_{2y}^{\circ}V_{y/3}'''O_{3+y};\quad [Mn^{4+}] = 2\cdot y$$

LCMx ($x \leq 0.7$) samples:

$$La_{1-x}Ca_x'Mn_{1-x}Mn_x^{\circ}O_3 + {}^{y}/_{2}\cdot O_2 \rightleftarrows La_{1-x}Ca_x'V_{y/3}'''Mn_{1-x-2y}Mn_{x+2y}^{\circ}V_{y/3}'''O_{3+y};\ [Mn^{4+}] = x + 2\cdot y$$

LCMx ($x \geq 0.7$) samples:

$$La_{1-x}Ca_x'Mn_{1-x}Mn_x^{\circ}O_3 \rightleftarrows La_{1-x}Ca_x'Mn_{1-x+2y}Mn_{x-2y}^{\circ}O_{3-y}V_y^{\circ\circ} + {}^{y}/_{2}\cdot O_2;\ [Mn^{4+}] = x - 2\cdot y$$

For LCMx samples, the Mn^{4+} content depends on the synthesis conditions as well as on the substitution level. As the temperature, oxygen pressure, and time of calcination were the same for all these samples, the $[Mn^{4+}]$ concentration plotted as a function of the Ca content should show a linear variation. This behaviour was observed for $x > 0.4$ (Figure 8). Fairly similar results for Sr-substituted manganite have been reported in the literature by many authors.[14−39] These authors showed that the concentration of Mn^{4+} was mostly determined by the substitution level of La^{3+} by Sr^{2+} rather than the synthesis conditions. For $0 \leq x \leq 0.4$, the Mn^{4+} content calculated from the substitution of lanthanum by calcium is different from that determined by chemical analysis, which indicated a deviation from the stoichiometry of lowly substituted LCMx compounds. Indeed, both the substitution level and the creation of cationic vacancies contribute to the determination of the Mn^{4+} concentration (see equations above). The results given in Figure 8 show that the ability to form over-stoichiometric compounds in air at 700 °C decreases with increasing calcium content and mostly disappears at $x = 0.7$. For $x > 0.7$, substoichiometric LCMx compounds were formed, their defect structures explained by the presence of anionic vacancies.

The structural modifications studied by XRD as a function of excess oxygen y and substitution level x were corroborated to IR investigations on the number and position of characteristic absorption bands. The observed band locations were explained in terms of an inverse relationship between atomic separation and vibrational frequency, and the band widths and splitting by the degree of degeneracy of the absorption mode and the resulting departure from cubic symmetry. $LaMnO_{3+y}$ ($y \geq 0.14$) and LCMx ($x \leq 0.4$) are rhombohedral, and the ν_1 band is narrower than this band in the orthorhombic materials [i.e., $LaMnO_{3+y}$ ($y \leq 0.09$) and LCMx ($x \geq 0.5$)].

The displacement of the ν_1 band to lower frequencies (Table 3) could be explained by consideration of the Mn−O bond order concept. Indeed, in the schematic energy level diagram of ABO_3 perovskites[40] the e_g electrons are in antibonding orbitals and so the bond order would decrease with an increase in the number of e_g electrons. This accounts for the observed decrease in the stretching frequency with increasing Mn^{3+} ($t_{2g}^3e_g^{*1}$) concentration (i.e. with decreasing y values). These results are in agreement with those reported for $LaBO_3$ oxides [B = Cr (d^3); Mn (d^4); Fe (d^5)] for which vibrational frequencies were in the order $\nu_{Cr-O} > \nu_{Mn-O} > \nu_{Fe-O}$.[41]

From the d_{Mn-O} values (Table 3) it can be seen that the increase in d_{Mn-O} together with the decrease in y induces a decrease in the vibrational frequency of the Mn−O bonds. This would be in agreement with a decrease in the bond force constant. Since the vibration ν_1 is primarily motion of oxygen ions, it is reasonable to expect that there should be little difference between Mn^{3+}−O and Mn^{4+}−O spectra. The Mn^{4+}−O frequency is slightly higher than that of Mn^{3+}−O because of the smaller lattice size and the fact that Mn^{4+} has a higher charge, thus increasing the Mn−O force constant. Moreover, the observed distances d_{Mn-O} were compared to the ionic radius sums $r_{Mn} + r_O$, where r_O is the ionic radius of the oxide ion (1.40 Å)[23] and r_{Mn} is the average ionic radius of the manganese site in the deficient structure [(c) in Table 1]. The differences between theoretical and observed distances (Δ) are included in

Table 3. The negative Δ values probably reflect partial covalent bond character and this covalent character would be weaker for LM(T,10^{-4}) oxides.

The spectra of lowly substituted LCMx ($x \leq 0.4$) perovskites are similar to those of rhombohedral LM solids. The fair constancy of ν_1 band frequency in the vicinity of 605 cm^{-1} is in agreement with the constancy of the Mn^{3+}/Mn^{4+} ratio (Figure 8). These observations also show that a change in the cations in perovskite A sites from La, with a mass of 139, to Ca, with a mass of 40, has no effect on the internal stretching mode frequency of B−O bond. Consequently, it is reasonable that the spectral components associated with common structural elements, namely MnO_3 octahedra, of LM and LCMx with rhombohedral symmetry should be similar. However, the A−MnO_3 lattice vibration frequency, ν_3, which is beyond the range of the spectrometer, should necessarily be different. With increasing substitution level x, the deviation from ideal cubic symmetry increases together with the Mn^{4+} content in the Mn sub-lattice, resulting in a lattice shrinkage due to the smaller size of the tetravalent ion. Consequently, the degeneracy seems to be completely removed and the infrared absorption bands are split in some components.

Conclusion

$LaMnO_{3+y}$ and $La_{1-x}Ca_xMnO_{3\pm y}$ perovskites with wide ranges of y ($0.02 \leq y \leq 0.26$) and x values ($0 \leq x \leq 1$) have been obtained by thermal treatment of aqueous-decomposed precursors at different temperatures and under different oxygen pressures. The influence of oxygen excess content y and the substitution level x in lanthanum manganites over a wide range of concentrations on the Mn^{4+} content, the symmetry of the perovskite structure, the defect chemistry and the infrared absorption bands of the stretching and bending Mn−O bond has been studied. All samples showed a deviation from ideal cubic symmetry even for the highest Mn^{4+} contents. Their symmetries were described as rhombohedral for $LaMnO_{3+y}$ ($y \geq 0.14$) and $La_{1-x}Ca_xMnO_{3\pm y}$ ($x \leq 0.4$) and orthorhombic for $LaMnO_{3+y}$ ($y \leq 0.09$) and $La_{1-x}Ca_xMnO_{3\pm y}$ ($x \geq 0.5$). Through consideration of five limiting defect structure models, the situation with equal vacancies on both La and Mn sites was proposed for $LaMnO_{3+y}$ and $La_{1-x}Ca_xMnO_{3\pm y}$ ($x \leq 0.7$), while oxygen vacancies were favoured as the predominant defect in the oxygen deficient region [i.e. $La_{1-x}Ca_xMnO_{3\pm y}$ ($x > 0.7$)]. The linear decrease in the volume per unit formula of the Ca-doped and undoped lanthanum manganites as well as the absorption frequencies and profiles of infrared bands characteristic of Mn−O bond were correlated with the change in Mn^{4+} content.

The next question to be solved with these compounds is to evaluate the change in surface composition and its behaviour toward probe molecule adsorptions and catalytic activity in combustion reactions.

Experimental Section

$LaMnO_{3+y}$ and $La_{1-x}Ca_xMnO_{3\pm y}$ samples, with x ranging from 0.00 to 1.00, were prepared in polycrystalline form from aqueous solutions of lanthanum nitrate, manganese acetate (for $LaMnO_{3+y}$) and calcium nitrate (for $La_{1-x}Ca_xMnO_{3\pm y}$). The obtained solution, with La/Mn and La+Ca/Mn atomic ratios equal to 1, was stirred constantly for2 h. Upon removal of the excess solvent by heating at 70 °C in vacuo (17 Torr), a gel containing the metal in solid solution was formed. The gel was dried at 110 °C for 24 h and was then decomposed at 450 °C in air. This treatment enabled total elimination of organic and nitrate materials. The resulting black powder was heated at different temperatures ranging from 700 to 1000 °C and at three different partial oxygen pressures for $LaMnO_{3+y}$ and in air (P_{O_2} = 0.21 atm) at 700 °C for (La,Ca)$MnO_{3\pm y}$. Each solid was maintained at the desired temperature for 24 h. The sample was then rapidly cooled to room temperature.

Throughout this article, the formal notations of LM(T,P) and LCMx, respectively, are used. LM(T,P) corresponds to $LaMnO_{3+y}$ obtained at a temperature T (700, 800, 900, or 1000 °C) and oxygen pressure (10^{-4}, 0.21, or 1 atm) and LCMx corresponds to $La_{1-x}Ca_xMnO_{3\pm y}$ obtained at T = 700 °C and P = 0.21 atm.

X-ray powder diffraction (XRD) patterns were obtained with Cu-K_α radiation in a Kigaku goniometer. For unit cell determinations, the patterns were collected by step-scanning from 10 to 80° in 2θ, in increments of 0.05° and a counting of 4 s each step. Lattice constants were refined by the least-squares method with the aid of the SILEX program.

Infrared spectra were recorded with a Perkin−Elmer FT-IR Paragon 1000PC in the 2000−300 cm^{-1} spectral range. The substance (ca. 0.3 wt%) was mixed thoroughly with dry KBr and pressed into discs of 0.5 mm thickness and 10 mm in diameter.

The lanthanum, manganese, and calcium contents in the solids were determined by atomic absorption spectroscopy. The concentrations of Mn^{3+} and Mn^{4+} ions were determined by redox titration.[42,43]

The densities of the samples were obtained by determining the volume of a known amount of powder in a pycnometer by use of bromobenzene. The experiments were performed in a climate room with a temperature of 19−20 °C. About 4−5 g of powder was used for each measure.

Acknowledgments

We would like to thank Professor A. Belhadj Amara, Faculté des Sciences de Bizerte, for helpful discussion and experimental support. We are deeply indebted to Dr. F. B. Amor, Faculté des Sciences de Tunis, for performing the refinements of XRD patterns.

[1] F. S. Galasso, *Structure, properties and preparation of perovskite-type compounds*, Pergamon, Oxford, **1969**.
[2] J. B. Goodenough, *Progress in solid state chemistry* (Ed.: H. Reiss), Pergamon, Oxford, **1971**, vol. 5.
[3] B. Goodenough, J. M. Longo, in: *Landolt-Bodenstein, Numerical Data and Functional Data in Science and Technology, New series* (Ed.: K. H. Hellwege), **1970**, vol. 4a, p. 131.
[4] N. Gunasekaran, J. J. Carberry, R. Doshi, C. B. Alcock, *J. Catal.* **1994**, *146*, 583.
[5] R. J. H. Voorhoeve, J. P. Remeika, L. E. Trimble, A. S. Cooper, F. J. Disalvo, P. K. Gallager, *J. Solid State Chem.* **1975**, *14*, 395.

[6] J. G. McCarty, H. Wise, *Catal. Today* **1990**, *8*, 231.
[7] N. Yamazoe, Y. Teraoka, *Catal. Today* **1990**, *8*, 175.
[8] G. Kremnic, J. M. L. Nieto, J. M. D. Tascon, L. G. Tejuka, *J. Chem. Soc., Faraday Trans.* **1985**, *81*, 939.
[9] P. D. Petrolekas, I. S. Metcalfe, *J. Catal.* **1995**, *152*, 147.
[10] T. Nitadori, S. Kurihara, M. Misono, *J. Catal.* **1986**, *98*, 221.
[11] Y. Yao, *J. Catal.* **1975**, *36*, 266.
[12] R. J. H. Voorhoeve, *Adv. Mat. Catal.* **1977**, 129.
[13] H. Taguchi, M. Shimada, *J. Solid State Chem.* **1987**, *67*, 37.
[14] M. Gaudon, C. Laberty, F. Ansart, P. Stevens, A. Rousset, *Solid State Sc.* **2002**, *4*, 125.
[15] J. W. Stevenson, M. M. Nasrallah, H. U. Anderson, D. M. Sparlin, *J. Solid State Chem.* **1993**, *102*, 175.
[16] J. H. Kuo, H. U. Anderson, D. M. Sparlin, *J. Solid State Chem.* **1989**, *83*, 52.
[17] K. Knizek, Z. Jirak, E. Pollert, F. Zounova, S. Sratislav, *J. Solid State Chem.* **1992**, *100*, 292.
[18] H. Taguchi, N. Nigao, M. Shimada, *J. Solid State Chem.* **1992**, *97*, 476.
[19] J. L. Garcia-Munoz, J. Rodriguez-Carvayal, P. Lacorre, J. B. Torrance, *Phys. Rev. B* **1992**, *46*, 4414.
[20] M. Marezio, J. P. Remeika, P. D. Dernier, *Acta Crystallogr., Sect. B* **1982**, *24*, 1986−38.
[21] R. D. Shannon, *Acta Crystallogr., Sect. A* **1976**, *32*, 751.
[22] V. M. Goldschmidt, *Skr. Norske Vidensk. Akad.* **1926a**, no. 2, **1926b**, no. 8.
[23] A. Wold, R. J. Arnott, *J. Phys. Chem. Solids* **1959**, *9*, 176.
[24] B. C. Tofield, W. R. Scott, *J. Solid State Chem.* **1974**, *10*, 183.
[25] J. A. M. Van Roosmalen, E. H. P. Cordfunke, *J. Solid State Chem.* **1994**, *110*, 106.
[26] G. V. Subba Rao, C. N. R. Rao, J. R. Ferraro, *Appl. Spectrosc.* **1970**, *24*, 436.
[27] J. T. Last, *Phys. Rev.* **1957**, *105*, 1740.
[28] G. Blasse, *J. Inorg. Nucl. Chem.* **1975**, *37*, 1347.
[29] S. D. Ross, *Inorganic Infrared and Raman Spectra*, Mc Graw-Hill, London, **1972**, p. 108.
[30] J. Nakagawa, A. Tsushida and Tshimanouchi, *J. Chem. Pys.* **1976**, *47*, 982.
[31] C. H. Perry, E. F. Young, *J. Appl. Phys.* **1967**, *38*, 4616.
[32] A. S. Barker, J. A. Ditzenberger, H. Guggenheim, *Phys. Rev.* **1968**, *175*, 1180.
[33] J. A. Alonso, M. J. Martinez-Lope, M. T. Casais, *Eur. J. Solid State Inorg. Chem.* **1996**, *33*, 331.
[34] M. Verelst, N. Rangavittal, C. N. Rao, A. Rousset, *J. Solid State Chem.* **1993**, *104*, 74.
[35] H. Tagichi, S. Matsu-ura, M. Nagao, T. Choso, K. Tabata, *J. Solid State Chem.* **1997**, *129*, 60.
[36] J. B. A. Elemans, B. Van Laar, K. R. Van Der Veen, B. O. Loostra, *J. Solid State Chem.* **1971**, *3*, 238.
[37] M. Hervieu, R. Mahesh, N. Ragavittal, C. N. R. Rao, *Eur. J. Solid Stae Chem.* **1995**, *32*, 79.
[38] F. A. Kröger, *The chemistry of imperfect crystals*, North Holland, Amsterdam, **1964**.
[39] A. Chakraborty, S. P. Devi, S. Roy, H. S. Maiti, *Mater. Lett.* **1994**, *20*, 63.
[40] J. B. Goodenough, *Les Oxydes des métaux de transition*, Gauthier-Villars Paris, Bruxelles, Lausannes, Montréal, **1973**, p. 253.
[41] P. Ganguly, N. Y. Vasanthacharya, *J. Solid State Chem.* **1986**, *61*, 164.
[42] Y. Takeda, S. Nakai, N. Imanishi, C. Q. Shen, O. Yamamoto, *Mat. Res. Bull.* **1991**, *26*, 153.
[43] K. S. Chan, J. Ma, S. Jaenicke, G. K. Chuah, J. L. Lee, *Appl. Catal. A* **1994**, *107*, 201.

Received January 14, 2003

